Separating ENSO and NAO signatures in the North Atlantic

Bianca Mezzina[1], Javier García-Serrano[1,2], Froila M. Palmeiro[1], Ileana Bladé[2]

[1]Barcelona Supercomputing Center (BSC), Barcelona, Spain
[2]Group of Meteorology, Universitat de Barcelona (UB), Barcelona, Spain

bianca.mezzina@bsc.es

Introduction

OBJECTIVE: use reanalysis and atmospheric models to investigate the ENSO teleconnection and dynamics versus internal variability in the North Atlantic.

The impact of ENSO on the **North Atlantic-European (NAE) sector**, a key factor for seasonal predictions, is still debated. ENSO-related signals in this region are difficult to detect because of the large internal variability.

▸ The wintertime ENSO signature projects on a **"NAO-like" pattern** in mean sea-level pressure (mslp), but it's essential to **distinguish ENSO from the internally-generated variability associated with the NAO**, linked to different dynamical processes.

▸ The target season of this study is **late winter (JFM)**, when the ENSO signal in this region is stronger and fully-established.

1. ENSO and NAO signals in reanalysis

To detect the ENSO- and NAO-related signals in reanalysis (NOAA-20CR), linear regression on two indices is used:

- **Niño3.4-index**: area-averaged SST anomalies (HadISST) over the Niño3.4 region (5°N-5°S; 170°W-120°W).
- **NAO-index:** 1st Principal Component (EOF) of mslp over the NAE domain (20°N-90°N; 90°W-40°E).

▸ Over the North Atlantic, the surface (mslp) wintertime signature of ENSO (**Fig.1c**) shows a **dipolar structure** that resembles the NAO (**Fig.1d**).

▸ The regression of z200 on the Niño3.4-index shows the well-known troposhperic **wavetrain** associated with ENSO (**Fig.1b**; *DeWeaver and Nigam, 2002; Bladé et al., 2008*).

▸ The regression of z200 on the NAO-index projects on the **circumglobal waveguide pattern** (**Fig.1b**; *Branstator, 2002*).

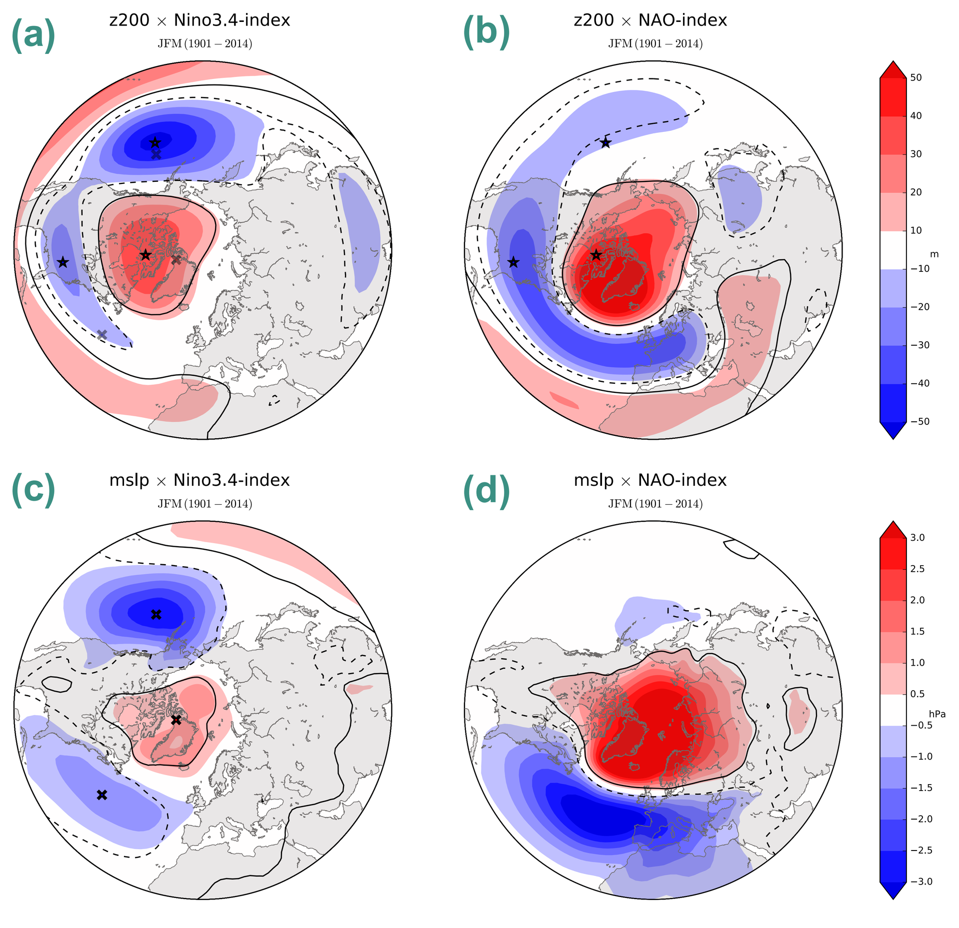

Figure 1. *Top:* linear regression of mslp anomalies on (a) Niño3.4-index and (b) NAO-index. *Bottom:* linear regression of z200 anomalies on (c) Nino3.4-index and (d) NAO-index. Contours indicate 95% significance. NOAA-20CR, JFM, 1901-2014.
✖: approximate center of ENSO anomalies in mslp.
★: same, but for z200.

2. Disentangling ENSO and NAO dynamics

Transient-eddy diagnostics are used to separate the dynamics linked to ENSO and the NAO.

The **eddy momentum flux** (u'v') at 200 hPa is computed from daily data using the 24-h filter (*Wallace et al., 1988*) and regressed on the two indices.

▸ ENSO mainly affects the storm-tracks in the North Pacific (**Fig.2a**), and consequently precipitation over North America (**Fig.2c**).

▸ In the North Atlantic, ENSO affects the **core of the eddy-driven jet** (**Fig.2a**) and has little impact on European precipitation (**Fig.2c**).

▸ The NAO shifts in latitude the **tail of the North Atlantic jet** and the storm-tracks (**Fig.2b**), leading to the characteristic **wet-dry dipole** over Europe (**Fig.2d**).

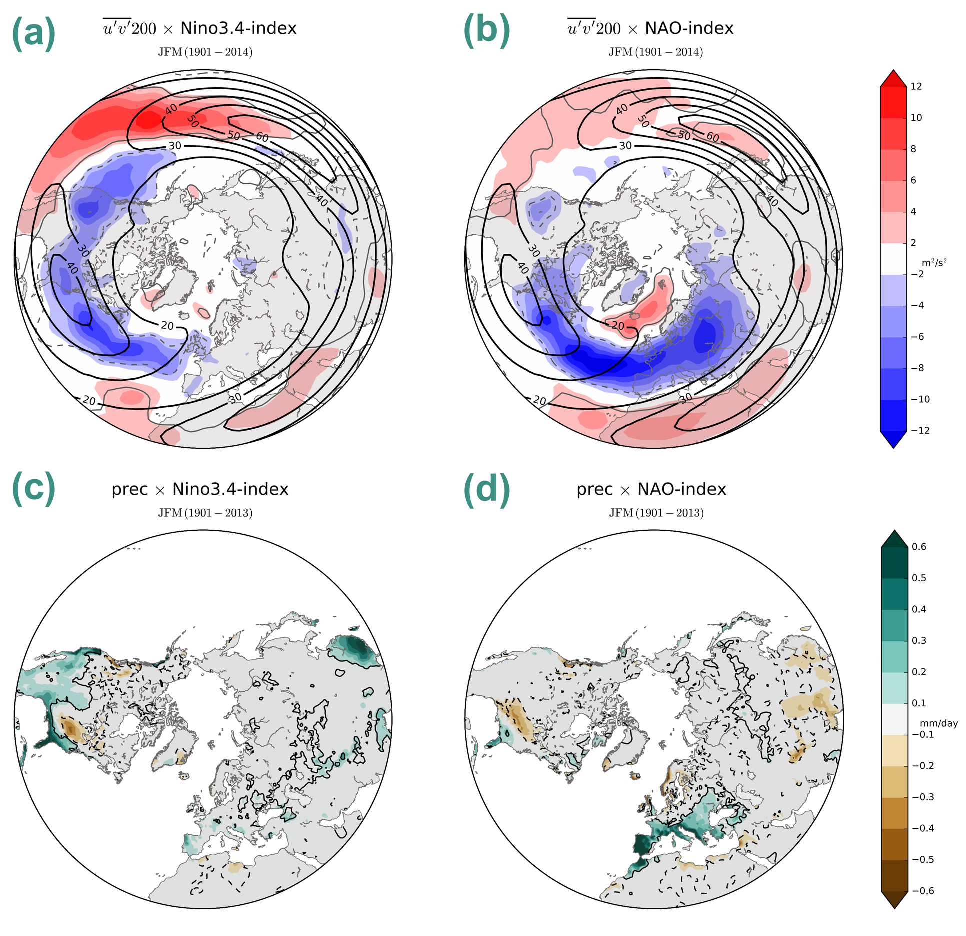

Figure 2. *Top:* linear regression of eddy momentum flux at 200 hPa on (a) Niño3.4-index and (b) NAO-index, with climatological u (thick contours). NOAA-20CR, JFM, 1901-2014. *Bottom:* linear regression of precipitation anomalies on (c) Niño3.4-index and (d) NAO-index. Contours indicate 95% significance. GPCC, JFM, 1901-2013.

3. Dynamics of the vertical structure

The vertical patterns of geopotential height anomalies over the North Atlantic are compared, along 35° N.

▸ ENSO shows a **westward tilt with height** (**Fig. 3a**, contours), also evident in **Figs. 1a, b**.

▸ A more **barotropic** structure characterizes the NAO anomalies (**Fig. 3b**, contours).

The **zonal-eddy heat flux** v*T* is a measure of vertical propagation of wave activity.

▸ Positive v*T* anomalies dominate the ENSO pattern (**Fig. 3a**, shading), indicating **upward wave-propagation**, consistent with the westward tilt.

▸ The NAO is associated with mixed v*T* anomalies, mainly confined in the lower troposphere (**Fig. 3b**, shading).

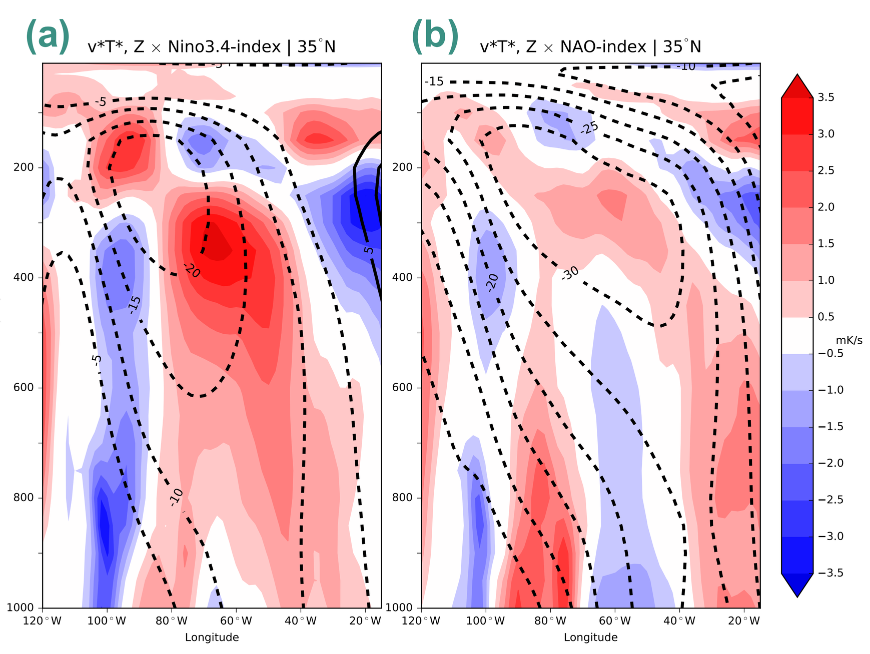

Figure 3. Cross sections at 35°N. *Contours:* linear regression of geopotential height anomalies on (a) Niño3.4-index and (b) NAO-index. *Shading:* same, but for v*T*. NOAA-20CR, JFM, 1901-2014.

4. Forced and internal variability in AGCMs

The ICTP AGCM (**SPEEDY**) is run with prescribed SSTs from observations (HadISST) to produce a 10-member ensemble (1901-2014). The SST-forced and internal variability are estimated as:

- **Forced:** 1st EOF of the ensemble-mean mslp in the Northern Hemisphere (**Fig. 4a**).
- **Internal:** 1st EOF of mslp residuals around the ensemble mean, in the NAE (**Fig. 4b**).

The corresponding principal components are used as indices to compute linear regression maps of the "forced" and "internal" components, without a priori involving ENSO and the NAO (*Zhang et al., 2016*).

▸ The SST-forced patterns resemble the observed regressions on the Niño3.4-index, both at surface (*cf.* **Figs. 4c, 1c**) and in the upper troposhere (*cf.* **Figs. 4a, 1a**), where the the extratropical wavetrain response to ENSO is evident.

▸ The **dominant role of ENSO in the forced variability** is confirmed by the regression map of SST anomalies (**Fig. 4e**); correlation with Niño3.4-index: 0.87.

▸ The leading mode of the **internally-generated variability** in mslp shows the **dipolar pattern of the NAO** (*c.f.* **Figs. 4d, 1d**); the NAO hemispheric signature at upper levels is also evident (*c.f.* **Figs. 4d, 1d**).

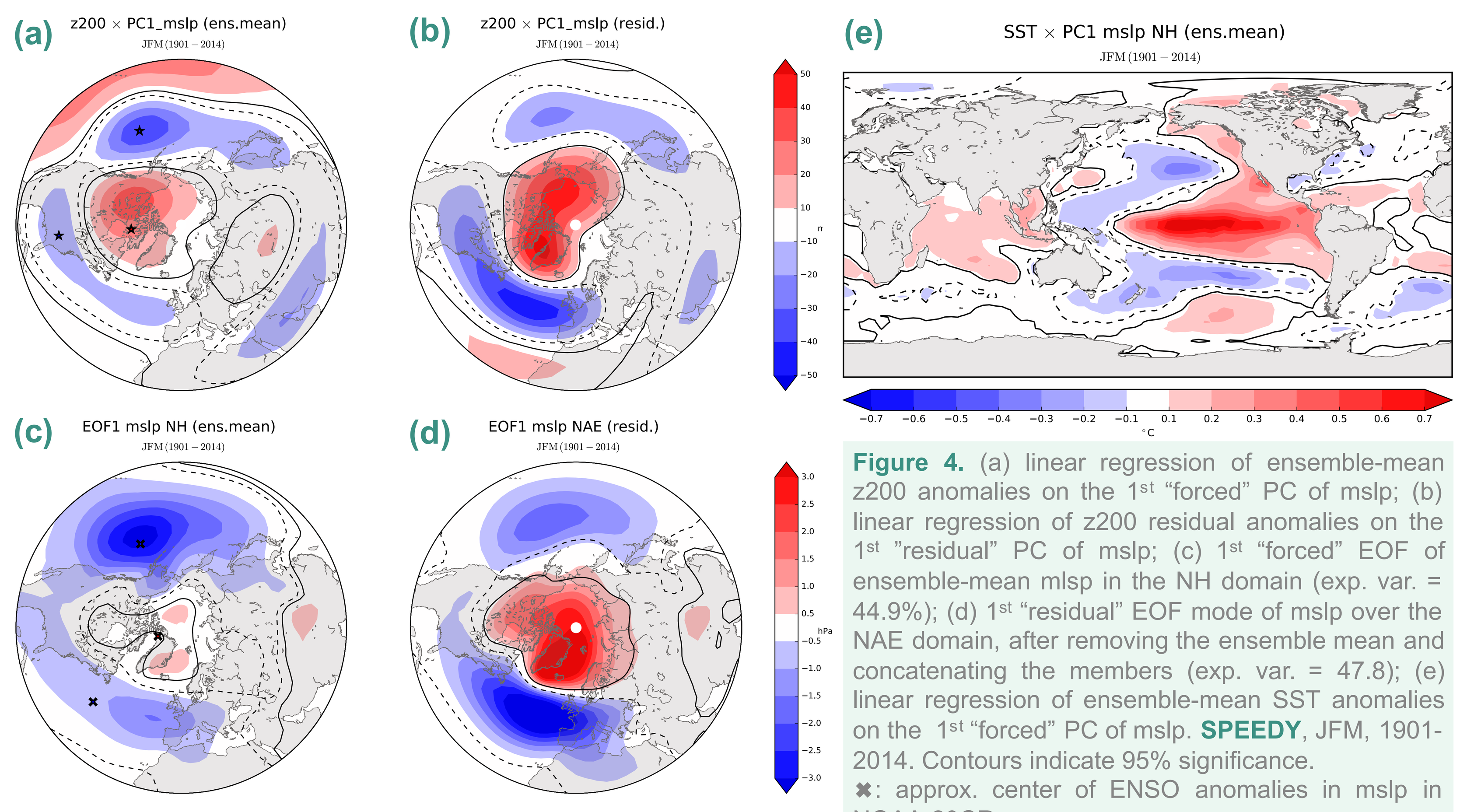

Figure 4. (a) linear regression of ensemble-mean z200 anomalies on the 1st "forced" PC of mslp; (b) linear regression of z200 residual anomalies on the 1st "residual" PC of mslp; (c) 1st "forced" EOF of ensemble-mean mlsp in the NH domain (exp. var. = 44.9%); (d) 1st "residual" EOF mode of mslp over the NAE domain, after removing the ensemble mean and concatenating the members (exp. var. = 47.8); (e) linear regression of ensemble-mean SST anomalies on the 1st "forced" PC of mslp. **SPEEDY**, JFM, 1901-2014. Contours indicate 95% significance.
✖: approx. center of ENSO anomalies in mslp in NOAA-20CR.
★: same, but for z200.

The analysis is repeated using the **ECMWF ERA-20CM model integrations**, a set of runs of the IFS AGCM with similar experimental set-up (prescribed forcing from HadISST), length (1901-2010) and number of members (10).

▸ The two models have different resolution (T30L8 in SPEEDY vs. T159L91 in IFS) and features, but the **results are similar** (*cf.* **Figs. 4, 5**).

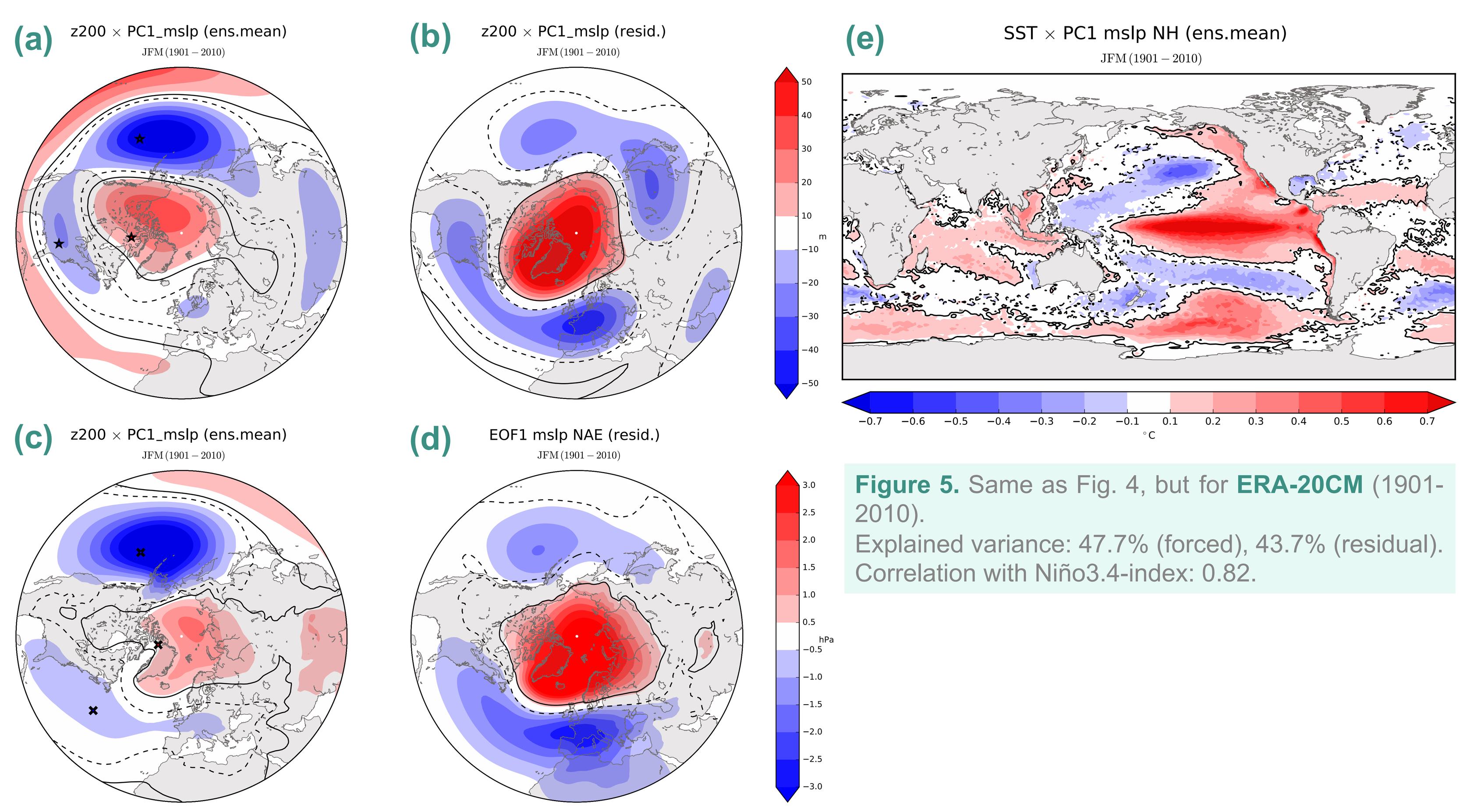

Figure 5. Same as Fig. 4, but for **ERA-20CM** (1901-2010).
Explained variance: 47.7% (forced), 43.7% (residual).
Correlation with Niño3.4-index: 0.82.

Key Messages

- **The late-winter ENSO teleconnection in the NAE is dynamically distinct from the NAO.**
- **The ENSO surface signature should be interpreted and referred to as "dipole-like" instead of "NAO-like"** (*García-Serrano et al. 2011*).
- **Considering the upper levels is fundamental to diagnose the different dynamics involved.**
- **The extratropical ENSO teleconnection in late-winter dominates the SST-forced variability in the Northern Hemisphere.**
- **The NAO controls the internally-generated (unforced) variability in the NAE region, as expected.**

References

Branstator, G., 2002: *Circumglobal Teleconnections, the Jet Stream Waveguide, and the North Atlantic Oscillation.* J. Clim., 15, 1893–1910.

Bladé, I., M. Newman, M. A. Alexander, J. D. Scott, 2008: *The Late Fall Extratropical Response to ENSO: Sensitivity to Coupling and Convection in the Tropical West Pacific.* J. Clim., 21, 6101–6118.

DeWeaver, E. and S. Nigam, 2002: *Linearity in ENSO's Atmospheric Response.* J. Clim., 15, 2446–2461.

García-Serrano, J., B. Rodríguez-Fonseca, I. Bladé et al., 2011: *Rotational atmospheric circulation during North Atlantic-European winter: the influence of ENSO.* Clim Dyn., 37,1727–1743.

Wallace, J.M., G. Lim, and M.L. Blackmon, 1988: "Relationship between Cyclone Tracks, Anticyclone Tracks and Baroclinic Waveguides". J. Atmos. Sci., 45, 439–462.

Zhang, T., M.P. Hoerling, J. Perlwitz, and T. Xu, 2016: *Forced Atmospheric Teleconnections during 1979–2014.* J. Clim. 29, 2333–2357.

Barcelona Supercomputing Center
Centro Nacional de Supercomputación

Universitat de Barcelona

This work has been supported by the Spanish MINECO-funded DANAE Project (CGL2015-68342-R).

Gobierno de España
Ministerio de Economía y Competitividad